unclassified

SECURITY CLASSIFICATION OF THIS PAGE *(When Data Entered)*

REPORT DOCUMENTATION PAGE

READ INSTRUCTIONS BEFORE COMPLETING FORM

1. REPORT NUMBER: SAIC-84-1428/PRI-86	2. GOVT ACCESSION NO.
3. RECIPIENT'S CATALOG NUMBER	
4. TITLE *(and Subtitle)*: Profile of a Relativistic Electron Beam Propagated through a Linear Wiggler and an Axial Guide Field	5. TYPE OF REPORT & PERIOD COVERED: preprint, technical report
6. PERFORMING ORG. REPORT NUMBER	
7. AUTHOR(s): B. Hafizi, G. L. Francis, R. E. Aamodt	8. CONTRACT OR GRANT NUMBER(s): N00014-79-C-0555
9. PERFORMING ORGANIZATION NAME AND ADDRESS: Science Applications International Corporation, Plasma Research Institute, 934 Pearl Street, Boulder, Colorado 80302	10. PROGRAM ELEMENT, PROJECT, TASK AREA & WORK UNIT NUMBERS: 61153N, RR011-07-03, NR 020-044
11. CONTROLLING OFFICE NAME AND ADDRESS: Office of Naval Research (Code 412), 800 N. Quincy Street, Arlington, VA 22217	12. REPORT DATE: December 1984
	13. NUMBER OF PAGES: 27
14. MONITORING AGENCY NAME & ADDRESS *(if different from Controlling Office)*	15. SECURITY CLASS. *(of this report)*: unclassified
	15a. DECLASSIFICATION/DOWNGRADING SCHEDULE

16. DISTRIBUTION STATEMENT *(of this Report)*

Approved for public release; distribution unlimited

17. DISTRIBUTION STATEMENT *(of the abstract entered in Block 20, if different from Report)*

18. SUPPLEMENTARY NOTES

19. KEY WORDS *(Continue on reverse side if necessary and identify by block number)*

relativistic electron beams
directed-beam quality
propagation through guide field and linear wiggler
density modulation
effective temperature

20. ABSTRACT *(Continue on reverse side if necessary and identify by block number)*

The density and parallel temperature of an electron beam passing through a magnetic guide field and a linear wiggler are determined as functions of distance from the anode. Starting with a given beam emittance and phase space distribution at the anode, single-particle orbits are employed to propagate the beam along the drift tube. Finite gyro-orbit effects induce substantial modulation in density. Additionally, the evolution of an initial spread in the parallel speed of the

DD FORM 1 JAN 73 1473 EDITION OF 1 NOV 65 IS OBSOLETE
S/N 0102-LF-014-6601

unclassified

SECURITY CLASSIFICATION OF THIS PAGE *(When Data Entered)*

block 20, Abstract, continued

electrons is sensitively dependent on the wiggler strength and contributes to further density fluctuation. The beam's parallel temperature, a critical factor in determining laser efficiency and gain, is found to increase significantly when the wiggler strength is raised.

SAIC-84-1428
PRI-86

December 1984

Profile of a Relativistic Electron Beam Propagated through a Linear Wiggler and an Axial Guide Field

B. Hafizi, G. L. Francis, R. E. Aamodt

Science Applications International Corporation
Plasma Research Institute
934 Pearl Street
Boulder, Colorado 80302

ABSTRACT

The density and parallel temperature of an electron beam passing through a magnetic guide field and a linear wiggler are determined as functions of distance from the anode. Starting with a given beam emittance and phase space distribution at the anode, single-particle orbits are employed to propagate the beam along the drift tube. Finite gyro-orbit effects induce substantial modulation in density. Additionally, the evolution of an initial spread in the parallel speed of the electrons is sensitively dependent on the wiggler strength and contributes to further density fluctuation. The beam's parallel temperature, a critical factor in determining laser efficiency and gain, is found to increase significantly when the wiggler strength is raised.

I. INTRODUCTION

In a free-electron laser, a beam of electrons of relativistic mass factor γ is passed through a magnetic wiggler field of wavelength λ resulting in emission of electromagnetic waves of wavelength $\lambda_{rad} \cong \lambda/(2\gamma^2)$ whose intensity is dependent on the beam density. For the most part, previous theoretical analyses of the free-electron laser instability have employed highly simplified models which assume this density is spatially uniform. Noting that any function of the constants of motion of a single electron is a steady state solution of the Vlasov equation, Davidson and Uhm[1] were the first to construct self-consistent equilibria for electron beams propagated in an axial guide field and a helical wiggler. The resulting spatial modulation of the electron density was determined for different choices of the functional dependence of the distribution function on the constants of motion.

In this paper, we examine the experimental situation in which the directional flux of electrons (and beam emittance) at the anode is specified and the beam is allowed to propagate through a drift tube immersed in a strong axial guide field and a linear (i.e., planar) wiggler. Using nonlinear particle orbits obtained earlier,[2] the distribution function of the electrons at any point along the drift tube is determined from the equation of continuity in phase space. The electron density is then obtained by an integration over momenta. Unlike the calculations in Ref. 1, an analysis using these orbits permits us to treat the case where there

is a resonance between the gyromotion of the electrons and the effective axial periodicity in parallel particle velocity induced by the wiggler. In addition, the radial dependence of the wiggler field is allowed for.

II. MATHEMATICAL ANALYSIS

We begin by choosing a rectangular coordinate system with the anode at its origin and the drift tube oriented along the positive z axis. In Ref. 2 it is argued that in the presence of an axial guide field it is natural to introduce the variables μ, θ, X, Y which are defined as follows:

$$\left.\begin{aligned} \mu &= (2m\,\Omega_o)^{-1}\,[(P_x + m\,\Omega_o y)^2 + p_y{}^2] \\ \theta &= \arctan\,[(P_x + m\,\Omega_o y)/p_y] \\ X &= x + (m\,\Omega_o)^{-1} p_y \\ Y &= -(m\Omega_o)^{-1} P_x \quad . \end{aligned}\right\} \qquad (1)$$

Here $\Omega_o \equiv qH_o/mc$ is the gyrofrequency of a particle with charge q and (rest) mass m in a magnetic field of intensity H_o. The canonical momenta P_x, p_y, p_z are related to the particle's velocity components v_x, v_y, v_z through the expressions

$$P_x = \gamma m v_x + (q/c)A_x = p_x + (q/c)A_x$$

$$p_{y,z} = \gamma m v_{y,z}$$

where

$$\vec{A} \equiv (A_x, A_y, A_z) = [-H_o y + \delta H k^{-1} \sin(kz)\cosh(ky), 0, 0]$$

is the vector potential of a linear magnetic wiggler of the form $[0, \delta H\cos(kz)\cosh(ky), -\delta H\sin(kz)\sinh(ky)]$ with wavelength $2\pi k^{-1}$ along the z-axis, superimposed on a guide field $(0,0,H_o)$. Note that in the absence of the wiggler field ($\delta H = 0$) the foregoing definitions of μ,θ,X,Y reduce to the usual expressions for the magnetic moment, gyroangle, and the x and y coordinates of the guiding center.

It is shown in Ref. 2 that for sufficiently small wiggler fields (measured by $\varepsilon \equiv \delta H/H_o$) the motion of the electrons can be locked onto a single resonance, with the particles strongly influenced by this resonance but mildly so by adjacent harmonics. This resonance condition has the form $\ell\dot{\theta}+k\dot{z} \cong 0$ for some integer ℓ, where $\dot{z}$ is the particle's axial velocity. It is further shown that in this case the motion is nonstochastic, and explicit integration of the equations of motion is possible. For free-electron laser applications it is imperative to limit the strength of the wiggler in order to avoid stochastic motion.

In the experiment conducted by Roberson et al.[3,4] at the Naval Research Laboratory, which provided the original motivation for this work, a current I_e of electrons ($\cong$500 A) is accelerated through a potential difference of 350 kV ($\gamma \cong 1.68$) before impinging on an anode of radius $R_o \cong 0.5$ cm and entering a 60 cm drift tube. From these numbers it follows that

$$\frac{I_e}{I_A} = \frac{\nu}{\gamma} \cong 2 \times 10^{-2}$$

where I_A is the Alfvén current, $\nu \equiv N(e^2/mc^2)$ is Budker's parameter, $N \equiv 2\pi \int_0^{R_o} rn(r)dr$ is the number of electrons per unit axial length, and

$n(x,y,z)$ is the electron density. With $\nu/\gamma << 1$, electric and magnetic self-field effects are measured by the dimensionless parameter[5] $\eta \equiv (2\gamma\omega_p^2/\Omega_o^2)[1-(v_z/c)^2]$ where

$$\omega_p \equiv (4\pi ne^2/m)^{\frac{1}{2}} \tag{2}$$

is the electron plasma frequency. For the NRL experiment $\eta \cong 1/2$. Further, in the experiment the magnetic field is allowed to build to its full value in a transition region preceding the drift tube entrance. Both the work described here and in Ref. 2 is idealized in that neither self-field effects nor the presence of a transition region are allowed for. In addition, because of uncertainties in the magnitude of various experimental parameters we shall, in what follows, estimate appropriate values when necessary.

The electron density at $\vec{r}$ is given by

$$n(\vec{r}) = \int d^3\vec{p}\ f(\vec{r},\vec{p}) \tag{3}$$

where $f(\vec{r},\vec{p})$, the electron distribution function, satisfies the conservation equation in six-dimensional phase space. Given this, it is clear that the electron density as a function of the distance along the drift tube in the steady state may be written

$$n(\vec{r}) = \int d^3\vec{p}\ f[\vec{R}(\vec{r},\vec{p}),\ \vec{P}(\vec{r},\vec{p})] \tag{4}$$

where $[\vec{R}(\vec{r},\vec{p}),\ \vec{P}(\vec{r},\vec{p})]$ is the phase space <u>orbit</u> of an electron which starts at the anode and reaches the point $(\vec{r},\vec{p}) \equiv (x,y,z,\vec{p})$ at the axial location z.

The final assumption of this work involves specifying the distribution function f at the anode. We shall assume

$$f(\text{anode}) = C\Theta(R_o-R)\delta[\hat{H}-(P_x^2+p_y^2+p_z^2)]\exp(-\phi) \qquad (5)$$

where C is a normalization constant, $\Theta(\cdot)$ is the Heaviside unit step function, R_o is the anode radius, $R \equiv (x^2+y^2)^{\frac{1}{2}}$ is the radial distance of the point (x,y,z) from the axis of the drift tube, $\hat{H}$ is related to the Hamiltonian $H = \gamma mc^2$ by

$$\hat{H} = H^2/c^2 - m^2c^2$$

$$= [P_x+m\Omega_o y-m\delta\Omega k^{-1}\sin(kz)\cosh(ky)]^2 + p_y^2+p_z^2$$

with $\delta\Omega \equiv q\delta H/mc$, and ϕ is given by

$$\phi = \frac{p_x^2 + p_y^2}{\bar{p}_\perp^2} + \frac{(p_z - p_b)^2}{\bar{p}_\parallel^2} \quad . \qquad (6)$$

In (6), $\bar{p}_\parallel$ and $\bar{p}_\perp$ are the spread in the parallel and perpendicular momenta of the electrons emerging from the anode, with the parallel momenta centered about the resonant value $p_b \equiv \ell m|\Omega_o|/k$ (Ref. 2). The Heaviside function in the expression for f indicates that the beam entering the drift tube has radius R_o and a uniform density over the anode area. The δ-function indicates that the beam is monoenergetic, with a fixed γ. The experimentally determined spread in the perpendicular speed is roughly given by $(\bar{p}_\perp/mc) \cong 0.08 - 0.24$; by a simple kinematical argument one finds

that $\bar{p}_{\parallel} \cong 1/2(\bar{p}_{\perp}^2/p_b)$, whence the spread in parallel speed is determined.

Given the distribution function and the (canonical) transformation (1), we proceed with the determination of $n(\vec{r})$. Since the Jacobian of (1) is $m|\Omega_o|$ (so that $dp_x dp_y dxdy = m|\Omega_o| d\theta d\mu dX dY$) we insert f into expression (4), integrate over p_z, and obtain

$$n(\vec{r}) = C\frac{m|\Omega_o|}{2} \int d\theta d\mu dX dY \Theta\{R_o - R[\vec{R}(\vec{r},\vec{p}), \vec{P}(\vec{r},\vec{p})]\}\ p_z^{-1}$$

$$\cdot \exp\{-\phi[\vec{R}(\vec{r},\vec{p}), \vec{P}(\vec{r},\vec{p})]\}\ \delta(x-X-\rho\cos\theta)\delta(y-Y+\rho\sin\theta), \tag{7}$$

where the factor 1/2 arises from the neglect of backward propagating particles, and the gyroradius $\rho \equiv (2\mu/m\Omega_o)^{\frac{1}{2}}$ relates the particle (x,y) and guiding-center (X,Y) coordinates via

$$X = x - \rho\cos\theta$$

$$Y = y + \rho\sin\theta \quad .$$

In order to complete the integration in (7) an explicit description of the particle orbit $[\vec{R}(\vec{r},\vec{p}), \vec{P}(\vec{r},\vec{p})]$ is needed. The calculation of these orbits is presented in the Appendix. Having determined them, (7) reduces to a double integral in μ and θ which can be evaluated using numerical techniques. Although μ appears to vary over a semi-infinite interval, the presence of a Gaussian-like integrand effectively reduces the region of integration to finite size. As z is varied, the size of this region is adjusted dynamically in order to include all significant

contributions of the integrand. Various mesh densities were employed in order to ensure convergence.

Having computed $n(\vec{r})$ it is straightforward to determine the parallel temperature T_z given by

$$T_z(\vec{r}) \equiv \frac{1}{n} \int d^3\vec{p} f(\vec{r},\vec{p}) \gamma m \left[\frac{p_z}{\gamma m} - V_z(\vec{r})\right]^2$$

where the mean parallel velocity V_z is

$$V_z(\vec{r}) \equiv \frac{1}{n} \int d^3\vec{p} f(\vec{r},\vec{p}) \frac{p_z}{\gamma m} \quad .$$

The quantity T_z is a measure of the spread in parallel velocities in the beam frame. In order that the electromagnetic radiation emitted by the electrons be as coherent as possible, and to allow operation in the collective (i.e., Raman) regime, T_z must be small.

Profiles of the density and parallel temperature for various wiggler field strengths and harmonics (given by ε and ℓ) are presented in the figures. These are reviewed in the next section. Plotted results are accurate to 1%.

III. DISCUSSION

In Fig. 1, the beam density (in arbitrary units) is plotted as a function of the axial distance z from the anode along the drift tube for $\varepsilon = 1/1024$. For the upper curve the observation point at which the density is measured has coordinates x = 0, y = 0.5 while the lower curve has x = 0, y = 1.0×10^{-2}. All linear dimensions are given in centimeters. The substantial density modulation evident in the upper curve can be understood by examining the nature of the particle orbits using Fig. 2. In this diagram, circle A represents the anode (chosen to have radius 1.2) and O is the observation point (coordinates x = 0, y = 0.5). (We use a somewhat larger anode radius in our numerical work in order to compensate for uncertainties in the experimental values of γ and the spread in $v_\perp$). Consider gyro-orbits which enclose circle R, pass through observation point O and have their guiding center on the y-axis (circle R_ℓ for example). Particles in such orbits necessarily move beyond the anode radius during part of their trajectory. Since the beam has little spread in parallel momentum by far the greatest number of particles have gyroradii equal to 0.453, that of particles exactly at resonance ($p_z = p_b = \ell m|\Omega_o|/k$). Circles R_ℓ and R_u are gyro-oribts that bound this most probable value, and are populated with $\sim 10^{-4}$ of the number of particles at resonance. As we move forward in space from the anode, the particles in the relevant orbits (denoted by the shaded regions) move outside A and the density at O falls. For $\ell = 2$, the resonance condition $\ell\dot{\theta} + k\dot{z} \cong 0$ implies that in one wiggler wavelength (3 cm) the particles complete about half of their

gyro-orbit and the density should be minimum. Over a distance of two wiggler wavelengths the particles return to their original locations (in the limit where all parallel momenta are identical) and the density is again at its peak.

Because a small spread in parallel momenta actually exists, particles completing their orbits return to their original positions at slightly different times, producing a smaller modulation of density evident in the shorter wavelength oscillations in the upper curve of Fig. 1 and the latter part of the lower curve.

Of course, there are other regions besides the shaded area in Fig. 2 which contribute to the plotted density modulations. We have simplified our discussion and diagram to keep the argument clear. By recalling, however, that the only significant gyroradii are approximately equal to 0.453 and that the observation point is O, it is easy to see that the only particles contributing to the density modulation lie in an appropriately expanded shaded region symmetrically placed about the y-axis. For instance, since the radius of circle L in Fig. 2 is 0.85, practially no particle with a guiding center lying on the y-axis to the left of O whose orbit passes through O moves out of A. Such a particle, therefore, does not contribute to the observed density depletion.

The wiggler acts to alter the speed of the particles as they move along the drift tube. By increasing the amplitude of the wiggler field an enhancement of the shorter-wavelength modulation seen in Fig. 1 is expected. This is clearly evident in Figs. 3 and 4 in which $\varepsilon = 1/128$ and $\varepsilon = 1/64$ respectively. It is this short-wavelength modulation that

is apparently discussed in Ref. 1, for in that work it is assumed there is no spread in the parallel momenta of the electrons. We further note that, since λ_{rad} is typically much smaller than the wiggler wavelength, the observed modulations in density not only should modify the gain but may also adversely affect the coherence and propagation characteristics of the emitted radiation.

In Fig. 5 the normalized parallel temperature $T \equiv (ck/\ell\Omega_o)^2 (\gamma T_z/mc^2)$ is plotted as a function of axial distance z for $\varepsilon = 1/1024$ and $\varepsilon = 1/128$. In both cases the observation point has coordinates $(x,y) = (0,0.5)$. One discerns the same six-centimeter modulation evident in the density plots. Again, these fluctuations are due to the spread in the parallel speeds of the particles and the fact that some particles periodically vacate the observation point and move outside of the nominal beam radius. The enhancement of the spread in parallel speeds caused by the wiggler is apparent by comparing the two curves. Note that, although the upper curve corresponds to a wiggler almost an order of magnitude stronger than the lower curve, both wiggler fields are, nonetheless, relatively weak. Furthermore, while the parallel temperature is seen to increase by about two orders of magnitude it is still not very large in absolute terms, roughly 10 keV at $z = 24$ cm, for $\varepsilon = 1/128$.

As is well-known,[6,7] the high gain and conversion efficiency associated with the operation of a free-electron laser in the Raman regime is predicated upon the availability of a cold electron beam having $(\delta\gamma_z)/\gamma_z \lesssim (\lambda/2\gamma^{3/2})(\omega_p/2c)$, which may be rewritten as

$$\frac{(\delta v_z)}{v_z} \lesssim \frac{\pi}{\gamma^{3/2}} \left(\frac{\omega_p}{\omega_{rad}}\right)\left(\frac{c}{v_z}\right)^2 \qquad (8)$$

Here ω_{rad} is the frequency of the emitted radiation, ω_p is defined in (2), and $\delta\gamma_z$ and δv_z denote the spread in $\gamma_z \equiv (1-v_z^2/c^2)^{-\frac{1}{2}}$ and v_z, respectively. With $(\delta v_z)/v_z)^2 \cong T_z/(\gamma m v_z^2)$, expression (8) can be rewritten in terms of the normalized parallel temperature as $T = (c/v_z)^4(\pi\omega_p/\omega_{rad})^2\gamma^{-1}$. For the NRL parameters[3,4] $T \cong 0.064$. Thus, for the two cases depicted in Fig. 5 the beam is sufficiently cold to allow operation in the Raman regime.

Figure 6 shows how the density modulations are affected by an increase in the parallel momentum of the particles. With the $\ell = 3$ harmonic resonant, $\gamma = 2.17$ and $\varepsilon = 1/128$ a typical gyroradius is the same as in the $\ell = 2$ case. For the upper curve in Fig. 6 the depth of modulation, defined as $(n_{max} - n_{min})/(n_{max} + n_{min})$, is very close to that of Fig. 3. This is to be expected since the gyroradius and anode radius are the same in both cases. Since $\ell = 3$, one also expects the density modulations to have a 9 cm wavelength, which is clearly evident in Fig. 6.

IV. CONCLUSION

The successful operation of a free-electron laser is strongly dependent on the quality of the electron beam employed. It is known that both the laser gain and the coherence of the radiated electromagnetic energy may be adversely affected by density fluctuations in the beam or spreads in parallel electron speed. In this paper we have examined an electron beam propagated through an axial guide field and a linear (i.e., planar) wiggler. By employing single particle orbits, the density and temperature of the beam as functions of distance from the anode have been determined. We present results which indicate that, unless care is taken, rather substantial modulations in beam density can be expected. In examining the density both on and off axis for various wiggler field strengths, we have found that these modulations increase both as the edge of the beam is approached, and as the wiggler strength is increased. This occurs for wigglers whose field strength is relatively small compared to the guide field. As a rough criterion for suppressing significant density fluctuations, we conclude that the electron gyroradius must be a small fraction of the beam radius. Moreover, the initial spread in the parallel speeds of the electrons must be small and the variation in this parallel speed induced by the wiggler must be comparable to this spread or smaller. This may result in the need to limit the strength of the wiggler, otherwise operation in the Raman regime may not be possible.

ACKNOWLEDGMENTS

We thank Dr. C. W. Roberson for making available to us the data referred to in this paper. This work was supported by the Office of Naval Research, U.S. Department of the Navy.

APPENDIX: SINGLE-PARTICLE ORBITS

In this appendix, the single-particle equations of motion are integrated and the particle orbit expressed as a function of the distance from the anode.

It is shown in Ref. 2 that if the wiggler field strength is small enough, so that the particle motion is influenced primarily by the ℓ-th resonance, then the equations of motion reduce to

$$\left(\frac{2\gamma}{\ell\Omega_o}\dot{I}\right)^2 + V_{eff}(I) = 0 \qquad \text{(A1)}$$

where

$$\mu = \frac{\ell^2 m\Omega_o}{k^2}(I+J) \quad ,$$

$$p_z = \frac{\ell m\Omega_o}{k}(I-1) \quad , \qquad \text{(A2)}$$

and

$$H_\ell = \left(\frac{k}{\ell m\Omega_o}\right)^2 \hat{H} - 1 - 2J \quad .$$

Here, the effective potential V_{eff} is given by

$$V_{eff}(I) \equiv (H_\ell - I^2)^2 - \left[\frac{2\varepsilon}{\ell^2} F_\ell(kY)\, \zeta \frac{dI_\ell}{d\zeta}\right]^2 \quad ,$$

with

$$\zeta \equiv k\rho = \ell[2(I+J)]^{\frac{1}{2}} \quad , \tag{A3}$$

$$F_\ell(x) \equiv \tfrac{1}{2}[\exp(x) - (-1)^\ell \exp(-x)] \ ,$$

and $I_\ell \equiv I_\ell(\zeta)$ the modified Bessel function of the first kind of order ℓ. Since the resonant value of the axial momentum equals $-\ell m\Omega_o/k$ (note $\Omega_o < 0$ for electrons) it follows from (A2) that $I=0$ at exact resonance.

In Ref. 2 several possible forms for the effective potential are sketched. For bounded motion of amplitude a and frequency α in a potential well having a minimum at $\hat{I}$, (A1) may be approximately integrated to obtain

$$I = \hat{I} + a \sin[\alpha(t-\tau)+\eta] \quad , \tag{A4}$$

where

$$\left.\begin{aligned} a &= \left[-2V_{eff}/\left(\frac{d^2V_{eff}}{dI^2}\right)\right]^{\frac{1}{2}}\Big|_{I=\hat{I}} \quad , \\ \alpha &= (\ell/2)\left(\frac{1}{2}\frac{d^2V_{eff}}{dI^2}\right)^{\frac{1}{2}}\Big|_{I=\hat{I}} \quad , \end{aligned}\right\} \tag{A5}$$

$$\sin(\eta) = \frac{I-\hat{I}}{a}$$

with the boundary condition that $I = I$ at $t = \tau$. (In our numerical work bounded potential wells are approximated by parabolas. This permits explicit determination of expressions (A4) and (A5)). Inserting (A4) into (A2) and using

$$p_z = \gamma m \frac{dz}{d\tau}$$

we obtain

$$Z = z + \frac{\ell\Omega_o}{\gamma k}(\hat{I}-1)(t-\tau) - \frac{\ell\Omega_o}{\gamma k\alpha} a\{\cos[\alpha(t-\tau)+\eta]-\cos(\eta)\} \quad . \tag{A6}$$

The equation of motion for the x-component of the guiding center may be expressed as[2]

$$\dot{X} = -\frac{\ell^2\Omega_o}{2\gamma k}\frac{F_{\ell+1}(kY)}{F_\ell(kY)}(H_\ell - I^2)$$

which, upon inserting (A4) and integrating, yields

$$X = X - \frac{\ell^2\Omega_o}{2\gamma k}\frac{F_{\ell+1}(kY)}{F_\ell(kY)}\left\{(H_\ell - \hat{I}^2 - \frac{a^2}{2})(t-\tau) + \frac{2a\hat{I}}{\alpha}\{\cos[\alpha(t-\tau)+\eta] - \cos(\eta)\}\right.$$

$$\left. + \frac{a^2}{4\alpha}\{\sin[2\alpha(t-\tau)+2\eta] - \sin(2\eta)\}\right\} \quad . \tag{A7}$$

Recalling that $\dot{\theta} = \frac{\partial H}{\partial \mu}$ we obtain, to lowest order in ε,

$$\dot{\theta} = \frac{\Omega_o}{\gamma} + \frac{4\varepsilon}{\gamma m}\left(\frac{m\Omega_o}{2k}\right)^2 i^{\ell+1} F_\ell(i\xi_\ell)\, F_\ell(kY)\frac{\partial}{\partial \mu}\left(\zeta \frac{dI_\ell}{d_\zeta}\right)$$

where $\xi_\ell = \ell\theta + kz$. Integrating this one obtains

$$\Theta = \theta + \frac{\Omega_o}{\gamma}(t-\tau) + \ldots \tag{A8}$$

where the neglected terms are nonsecular and of order ε, or secular and higher order. Finally, noting that a and the oscillatory term tend to zero as $\varepsilon \to 0$, (A6) may be inverted to yield

$$t - \tau = \frac{\gamma k(Z-z)}{\ell\Omega_o(\hat{I}-1)} \quad . \tag{A9}$$

This may be inserted in (A4), (A7) and (A8) yielding the orbits needed to perform the integration in (7).

REFERENCES

1. R. C. Davidson and H. S. Uhm, J. Appl. Phys. 53, 2910 (1982).
2. B. Hafizi and R. E. Aamodt, Phys. Rev. A 29, 2656 (1984).
3. C. W. Roberson, J. Pasour, F. Mako, R. Gilgenbach and P. Sprangle, Bull. Am. Phys. Soc. 26, 1016 (1982); C. W. Roberson (private communication).
4. C. W. Roberson, J. Pasour, F. Mako, R. Lucey and P. Sprangle, Infrared and Millimeter Waves, Vol. 10, ed. K. J. Button (Academic, New York, 1983), p. 361.
5. R. C. Davidson and W. A. McMullin, Phys. Fluids 27, 1268 (1984).
6. A. Hasegawa, Bell Syst. Tech. J. 57, 3069 (1978).
7. S. C. Chen and T. C. Marshall, Phys. Rev. Lett. 52, 425 (1984).

FIGURE CAPTIONS

Fig. 1 Normalized density D as a function of the distance z (in cm) measured from the anode along the drift tube. Wiggler wavelength $2\pi/k$ = 3 cm, γ = 1.68, guide field H_o = 2.2 kOe, $\varepsilon \equiv \delta H/H_o$ = 1/1024, resonance harmonic number ℓ = 2, radius of anode R_o = 1.2 cm. Observation point for lower curve has coordinates (x,y) = $(0,10^{-2})$ cm; for upper curve (x,y) = (0,0.5) cm.

Fig. 2 Relationship between anode and typical gyro-orbits at observation point O with coordinates (x,y) = (0,0.5) cm.

Fig. 3 Normalized density D as a function of the distance z along the drift tube when ε = 1/128. Other parameters are the same as those in Fig. 1.

Fig. 4 Normalized density D as a function of the distance z along the drift tube when ε = 1/64. The observation point has coordinates (x,y) = $(0,10^{-2})$ cm. Other parameters are the same as those in Fig. 1.

Fig. 5 Normalized parallel temperature $T \equiv (ck/\ell|\Omega_o|)^2(\gamma T_z/mc^2)$ as a function of the distance z along the drift tube. For the upper curve $\varepsilon = 1/128$; the lower curve has $\varepsilon = 1/1024$. The observation points for both curves have coordinates (x,y) = (0,0.5) cm. Other parameters are the same as those in Fig. 1.

Fig. 6 Normalized density D as a function of the distance z along the drift tube when $\gamma = 2.17$, $\varepsilon = 1/128$ and the resonance harmonic number $\ell = 3$. Other parameters are the same as those in Fig. 1.

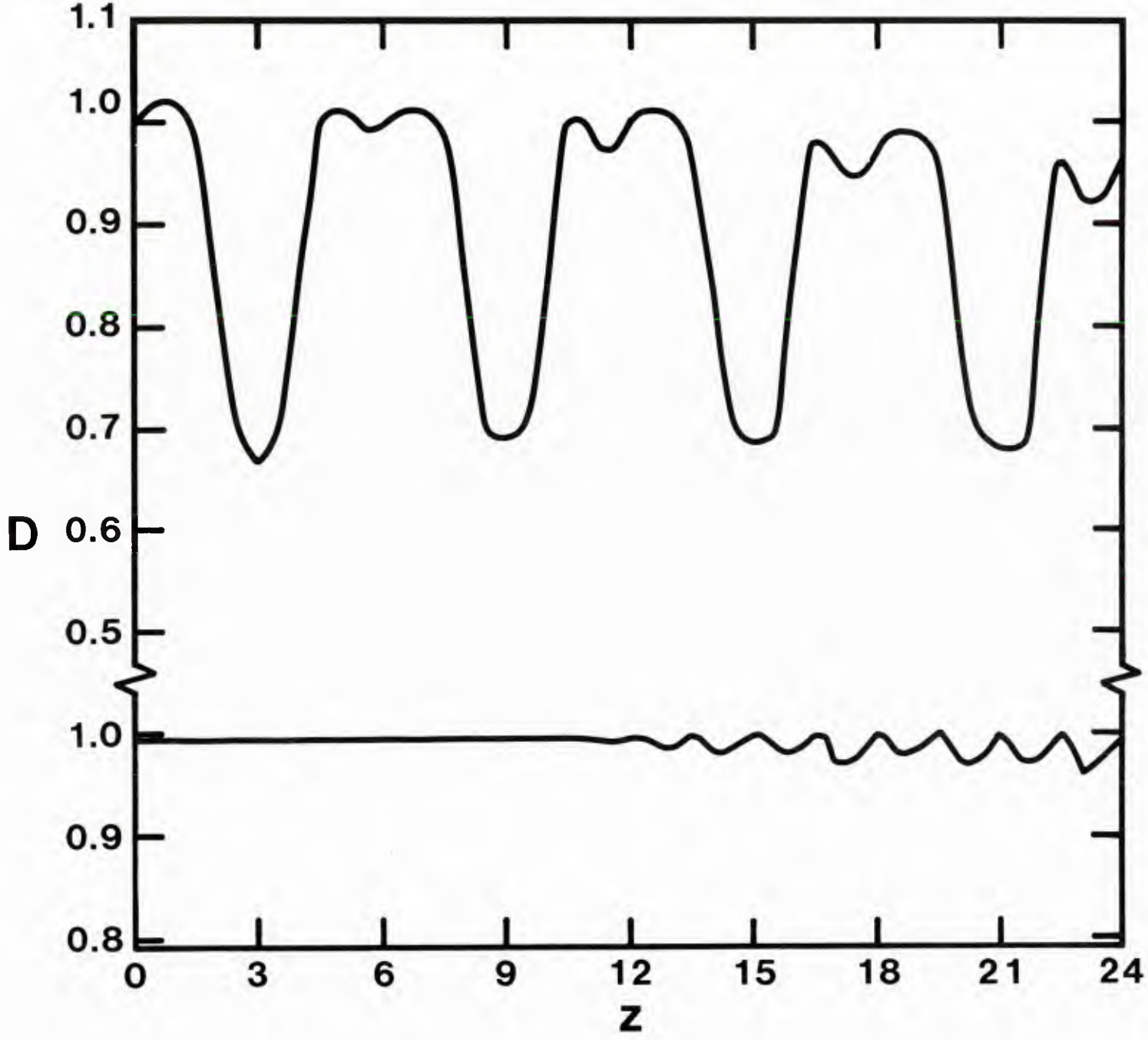

Fig. 1

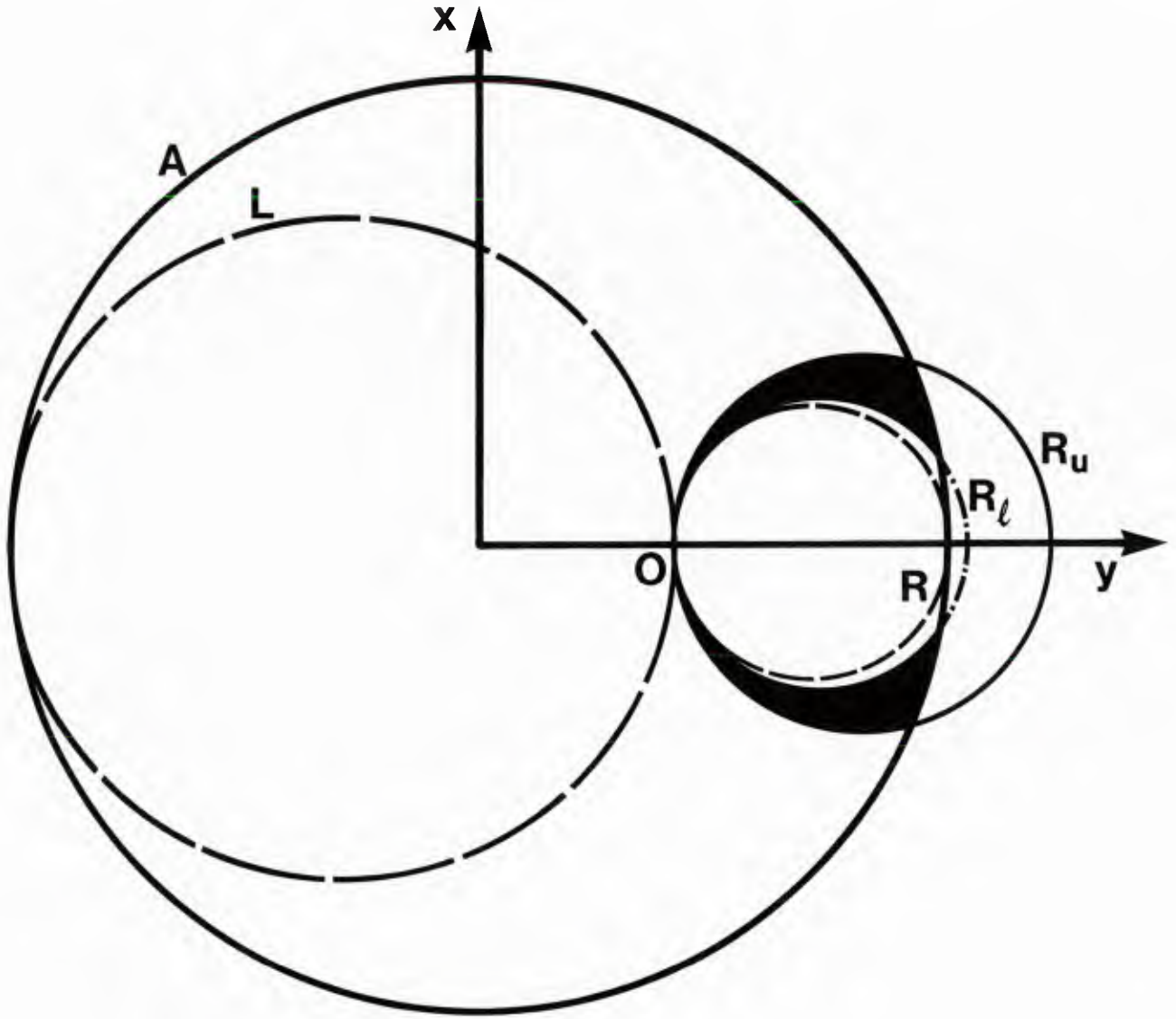

Fig. 2

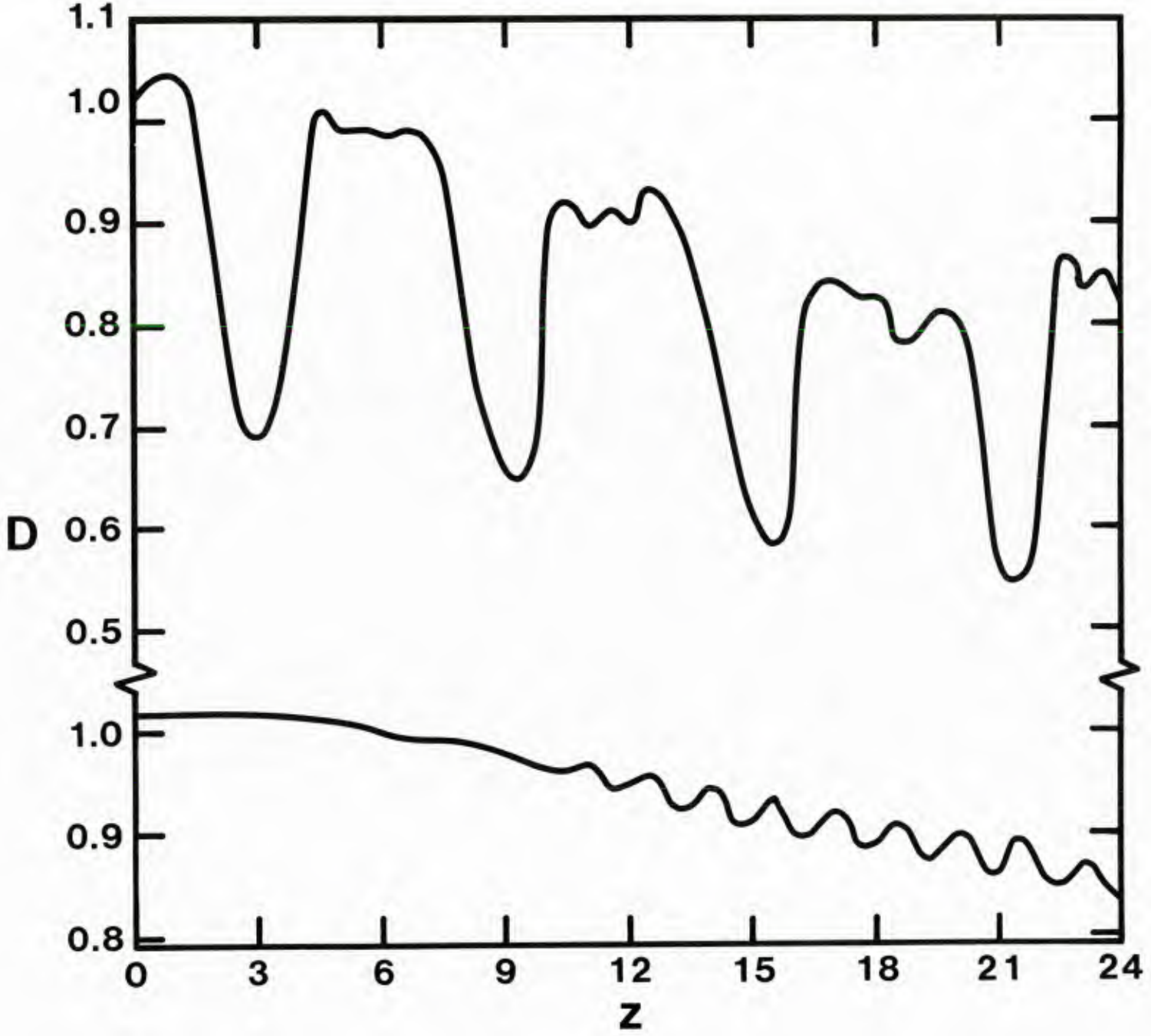

Fig. 3

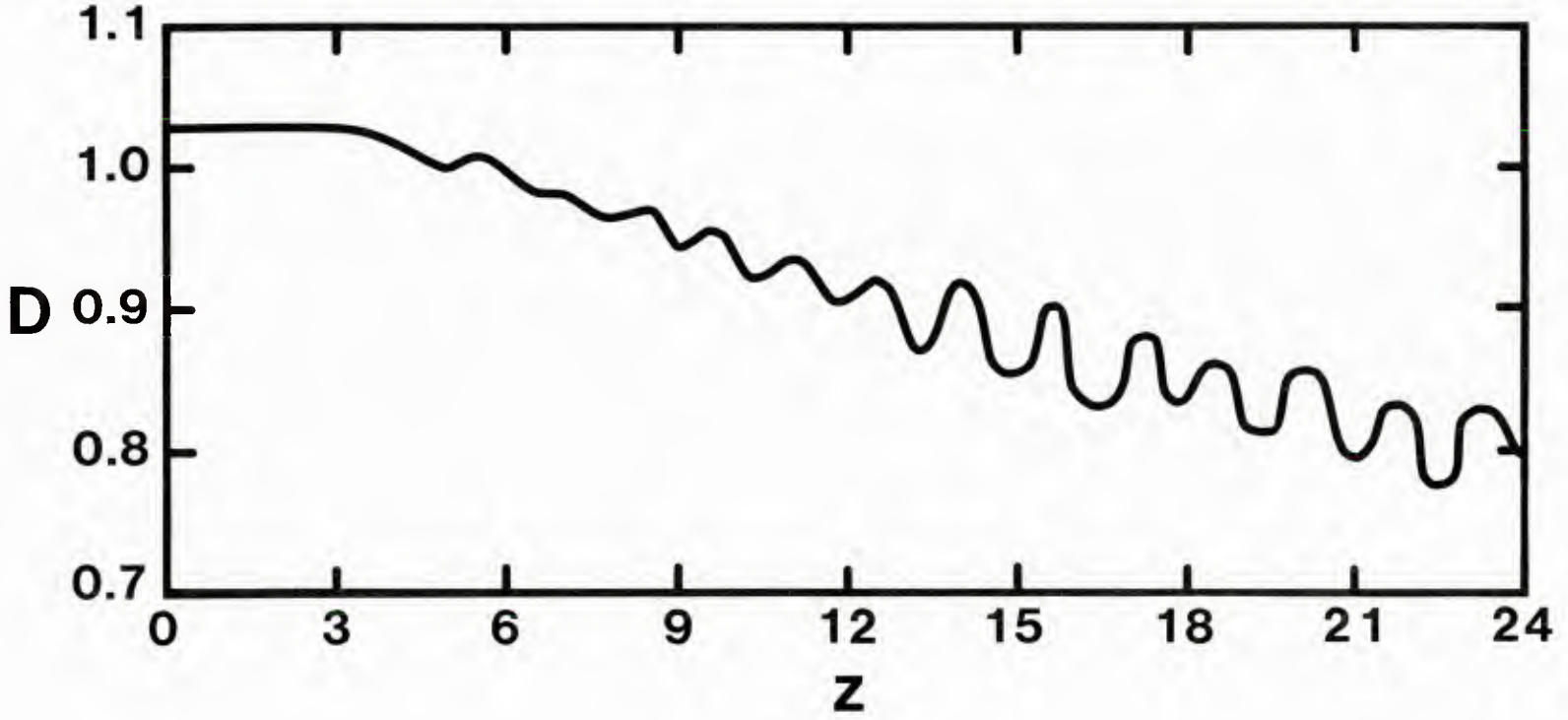

Fig. 4

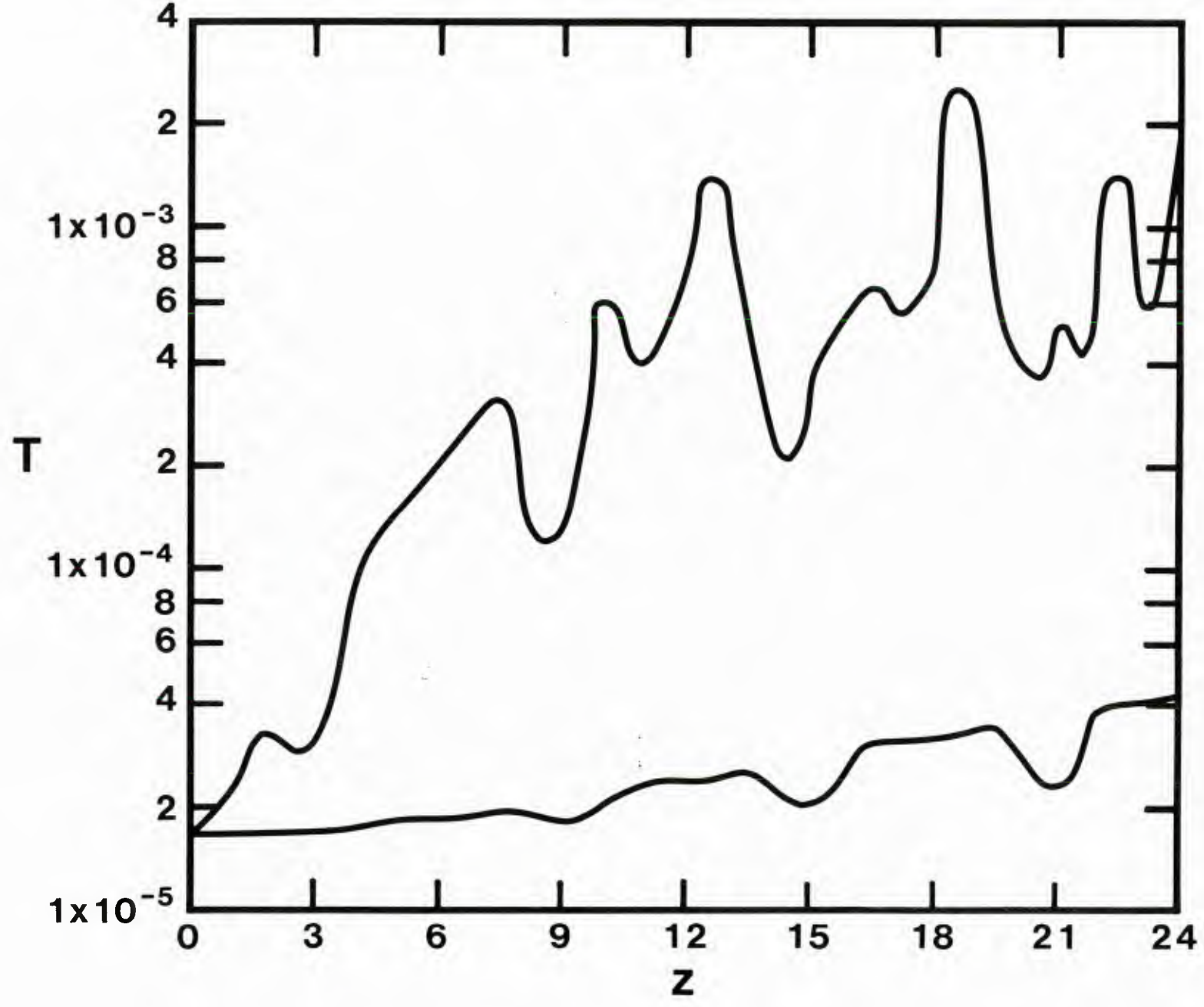

Fig. 5

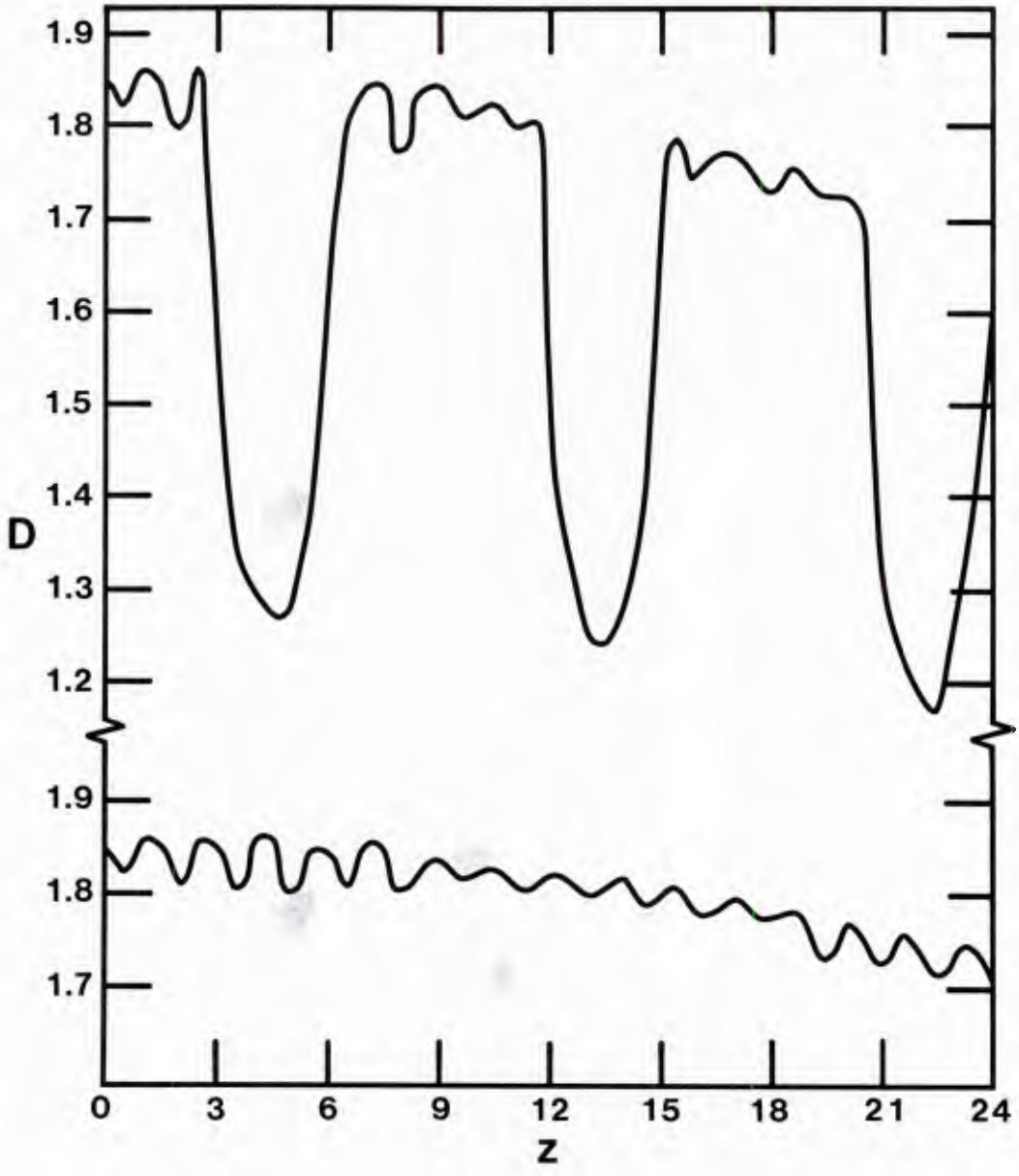

Fig. 6